Available online at www.sciencedirect.com
ScienceDirect
International Journal of Heat and Mass Transfer 51 (2008) 696–706
International Journal of HEAT and MASS TRANSFER
www.elsevier.com/locate/ijhmt

A numerical method for the Rubinstein binary-alloy problem in the presence of an under-cooled liquid

V.R. Voller *

Saint Anthony Falls Laboratory, Civil Engineering, University of Minnesota, Mississippi River at 3rd Avenue SE, Minneapolis, MN 55414, USA

Received 12 December 2006; received in revised form 24 April 2007
Available online 3 July 2007

Abstract

A fixed grid solution for tracking a moving solidification front controlled by coupled heat and mass transport in the presence of an under-cooled liquid is developed. A known closed form similarity solution for the solidification of a binary alloy in a one-dimensional domain is outlined. A previously reported enthalpy based model for this problem is presented and a novel numerical solution devised. Comparisons with the analytical solution show that the proposed numerical solution can produce high-fidelity predictions across a wide range of conditions including cases where the liquid becomes under-cooled.

Keywords: Binary alloy; Enthalpy method; Constitutional under-cooling; Analytical solution

1. Introduction

Solidification problems that exhibit a moving and sharp interface between the solid and liquid phases are computationally challenging. The key difficulty is the requirement to accurately track the solid–liquid interface as it moves over a discrete description of the problem domain. Many popular numerical solutions used to overcome this difficulty are based on the enthalpy formulation [1,2]. Such methods, dating back to the middle of the last century [3,4], are based on a governing equation that conserves the energy (enthalpy). This equation is valid throughout the problem domain (solid + liquid) and can be numerically solved, at each time step, on a fixed space grid. From the calculated nodal enthalpy field an auxiliary variable—the liquid fraction ($f = 1$ in liquid, $f = 0$ in solid)—can be extracted and used to track the movement of the solid–liquid interface [4–6]. Enthalpy methods have been extensively verified against alternative approaches for tracking solidification fronts, e.g., front fixing [7], deforming grids [8], and semi-analytical [9].

The classic solidification problem is the Stefan problem [1]. The problem is set in a one-dimensional semi-infinite domain $x^* \geqslant 0$ containing a single component (pure) liquid, super heated to a temperature T_0^* above the unique solidification temperature T_f^*. A solidified layer is advanced into the liquid by lowering and maintaining the temperature at the surface $x^* = 0$ to $T_{sur}^* < T_f^*$. This is a useful problem because, when the heat transfer is controlled by heat conduction alone, it can admit a closed similarity solution [1]; a solution that can be used to verify numerical solution approaches designed for more general cases.

An explicit time stepping enthalpy solution of the classic Stefan problem will (i) solve for the nodal enthalpy field at the new time level using the nodal temperature field from the previous time step and then (ii) use the updated nodal enthalpy field to calculate an updated nodal temperature field for use in the next time step. A key feature, that enables the updating of the nodal temperature field from the enthalpy, is that node points in the discretization where the phase change is occurring are readily identified. For example, assuming a single constant volumetric specific

* Tel.: +1 612 625 0764.
E-mail address: volle001@umn.edu

0017-9310/$ - see front matter © 2007 Elsevier Ltd. All rights reserved.
doi:10.1016/j.ijheatmasstransfer.2007.04.020

Nomenclature

c^*	volumetric specific heat [J/m^3 K]
c	normalized specific heat
C^+	is solute concentration [wt%]
C_0	initial solute concentration in the liquid [wt%]
C	concentration normalized by C_0
D^*	mass diffusivity [m^2/s]
D	normalized mass diffusivity
f	liquid fraction
H^*	volumetric enthalpy [J/m^3]
H	dimensionless enthalpy
h	dimensionless heat transfer coefficient
k	is the partition coefficient
Le	Lewis number [$=\frac{\alpha_l^*}{D_l^*}$]
l	a length dimension [m]
L^*	volumetric latent heat [J/m^3]
L	dimensionless latent heat
m	slope in phase diagram [K]
q^{H}	dimensionless heat flux
q^{C}	dimensionless solute flux
St	solutal Stefan number [$=-m_l C_0 \frac{c_l^*}{L^*}$]
s	location of the solid–liquid interface
T^*	temperature [K]
T	dimensionless temperature
T_{amb}	dimensionless ambient temperature
T^*_{equ}	equilibrium temperature [K]
T_{equ}	dimensionless equilibrium temperature
T^*_{f}	fusion temperature of solvent [K]
t	time
V	solute potential
x	space dimension

Greek symbols

α^*	thermal diffusivity [m^2/s]
α	normalized thermal diffusivity
λ	similarity variable

Superscripts

f	mixture value
i	solid–liquid interface value
new	new time level
*	quantity with dimension

Subscripts

i	node point counter
i_in	left face of control volume i
i_out	right face of control volume i
l	liquid phase
s	solid phase

heat c^*, a latent heat L^*, and setting the reference temperature for calculating the enthalpy as T^*_{f}, the phase change nodes can be identified by enthalpies falling in the range $c^*T^*_{\mathrm{f}} < H^* < c^*T^*_{\mathrm{f}} + L^*$; in one-dimensional problems there is never more than one node, in a given time step, that will satisfy this condition.

Moving away from the classic Stefan problem a more advanced solidification problem considers the solidification of multi-component alloys, e.g., see recent work by Voller and co-workers [2,10], and Ganguly and Chakraborty [11]. A standard test problem, the so-called "binary-alloy problem", involves the solidification of a binary alloy in the one-dimensional semi-infinite domain $x^* \geqslant 0$. Initially, the alloy is liquid with a uniform solute composition C_0 and temperature above the equilibrium liquidus temperature, i.e., $T^*_0 > T^*_{\mathrm{equ}}$, the liquidus line in the phase diagram (see schematic in Fig. 1). Solidification is nucleated by lowering and fixing the surface temperature to $T^*_{\mathrm{sur}} < T^*_{\mathrm{equ}}$. When the binary liquid solidifies there is a partitioning of the solute between the solid and liquid phases. As a result the movement of the solid–liquid interface is controlled by both heat and mass (solute) transport. As with the case of solidification of a pure liquid, if the heat and mass transport is controlled by diffusion, a closed form similarity solution can be found, Rubinstein [12] (see discussion in Alexiades and Solomon [13]).

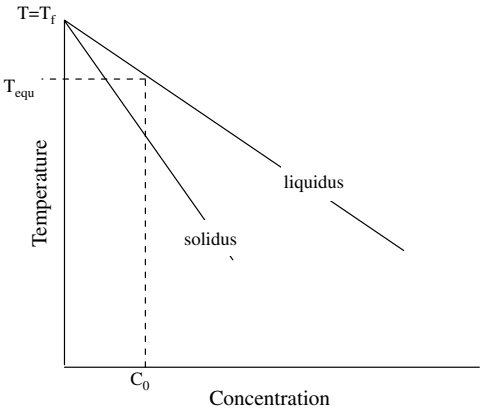

Fig. 1. Schematic of binary phase diagram.

An enthalpy based model and numerical solution of the one-dimensional binary-alloy problem has been presented by Crowley and Ockendon [14]. In this solution the unique node where the solid–liquid interface is located is, assuming a constant specific heat and a reference temperature $T^*_{\mathrm{f}} + mC_0$, identified by the nodal enthalpy falling in the range $c^*T^*_{\mathrm{equ}} < H^* < c^*T^*_{\mathrm{equ}} + L^*$. In contrast to the basic Stefan problem where the phase change temperature T^*_{f} is a fixed constant, the equilibrium temperature T^*_{equ} in this

condition depends on the current value of the solute concentration and hence varies from node to node and time step to time step. This necessitates the solution of a non-linear equation to update the nodal temperature field from the current enthalpy field. Crowley and Ockendon [14] use their enthalpy method to solve an example problem and show excellent agreement with the Rubinstein [12,13] similarity solution. In later work Voller [15] used an implicit time stepping version of the Crowley and Ockendon enthalpy model in conjunction with a variable time step to restricted the solid–liquid interface to coincide with a node point at each time step. The performance of this "node jumping" scheme matched that reported by Crowley and Ockendon [14].

Alexiades and Solomon [13] and Wilson et al. [16] have highlighted an important shortcoming with the Crowley and Ockendon enthalpy solution. When the Lewis number (the ratio of thermal to solute diffusivity in the liquid phase) is large, the solute rejected into the liquid as the solid forms is not easily removed from the region ahead of the solid–liquid interface. This can lead to a situation known as constitutional under-cooling [17] in which there is a region ahead of the interface where the equilibrium temperature, calculated by substituting the solute concentration into the liquidus line of the phase diagram, is above the real temperature, i.e., $T_{\text{equ}} > T$, see Fig. 2. This has two possible consequences. (1) The operation of the Crowley–Ockendon method may fail since, in the region of constitutional under-cooling, there could be a number of nodes where $T^*_{\text{equ}} < H^* = c^*T^* + L^* < T^*_{\text{equ}} + L^*$ and as a result a unique node associated with the solid–liquid interface cannot be identified. (2) In a physical setting, any small solid imperfection forming on the interface will find itself in a local environment favorable for further growth, resulting in a break down of the solid–liquid interface into a mushy region, where, at the scale of the problem, distinct solid and liquid regions cannot be identified. Wilson et al. [16] take account of both of these consequences in developing a numerical solution that is able to handle the formation of a mushy region. In essence the use of this modified solution assumes that once a region of constitutional under-cooling is formed the sharp solid–liquid interface will break down into a mushy region. This is a reasonable assumption if the scale of the problem—defined by the width of the domain normal to the growth direction—is much larger than the characteristic length scale of the solid–liquid morphology in the mushy region. On the other hand, if the scale in the normal direction is small, i.e., the solidification domain is an insulated thin "slot" like geometry, then it may be possible to retain a sharp-solid liquid interface in the presence of liquid under-cooling. In fact, if the thickness of the slot is less than the critical wave length calculated by the Mullins and Sekerka interface stability theory [18], a sharp-planar interface will be maintained. Hence, under the correct physical situation it is reasonable to assume a sharp-interface in the presence of liquid under-cooling.

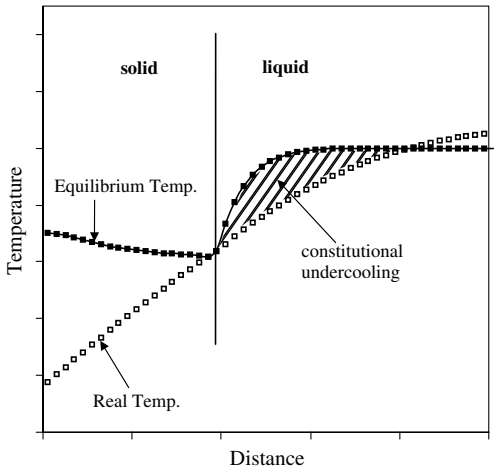

Fig. 2. Region of constitutional under-cooling.

The objective of this paper is to extend previous enthalpy methods to solve binary-alloy problems that involve a sharp-interface in the presence of an under-cooled liquid. The proposed extension of the enthalpy method is related to a recent modification of the Crowley and Ockendon [14] scheme that has been used to simulate the dendritic growth of equiaxed dendritic crystals in initially under-cooled melts [19]. In contrast to this work, the solution of the binary-alloy problem—as stated above—does not require incorporation of surface-tension induced under-cooling on the solid–liquid interface. The solution of the binary-alloy problem does, however, require consideration of key features that are not treated in the previous enthalpy simulation of equiaxed crystal growth [19]; in particular, a fixed temperature boundary condition and different physical properties between solid and liquid phases. These features result in additional numerical complexity, the former requires a treatment of heat and solute transport in the solid phase, the later requires handling of the discontinuous properties across the solid–liquid interface. Incorporating an ability to handle a fixed temperature boundary condition and discontinuous properties, even in the absence of surface-tension or kinetic under-cooling, represents a contribution in current efforts toward a complete model of crystal growth processes.

In light of the above discussion, the development of the new enthalpy method for solving the binary-alloy problem in the presence of an under-cooled melt is justified on two counts. (1) It is physically possible to maintain a sharp interface in the presence of under-cooling and hence a solution may have practical value. (2) The numerical developments required will improve and verify the capabilities of fixed grid enthalpy methods for the more general solidification moving boundary problems related to crystal growth.

In the next section the governing equations and the Rubinstein [12,13] similarity solution are outlined and particular limit cases are noted. Then a version of the Crowley and Okendon [14] enthalpy model of binary alloy solidification is presented. A new enthalpy solution that can

handle discontinuous thermal properties—in particular specific heat—and maintain a sharp interface in the presence of liquid under-cooling is developed. The proposed solution method is tested by comparing with the Rubinstein solution for three cases, (i) no under-cooling during solidification, (ii) the appearance of constitutional undercooling during solidification, and (iii) solidification into an initially under-cooled melt. To the author's knowledge the solution of the later two problems is the first time that an enthalpy solution to the binary alloy problem in the presence of liquid undercooling has been presented.

2. The binary alloy problem and Rubinstein [12,13] solution

2.1. Parameters and variables

The following scalings and dimensionless numbers will be used throughout this work

$$\begin{aligned} &H=\frac{H^*}{L^*},\quad T=\frac{T^*-T_{\mathrm{f}}^*-m_{\mathrm{l}}C_0}{L^*/c_{\mathrm{l}}^*},\quad C=\frac{C^+}{C_0},\\ &x=\frac{x^*}{l},\quad s=\frac{s^*}{l},\quad t=\frac{\alpha_{\mathrm{l}}t^*}{l^2},\quad \alpha=\frac{\alpha_{\mathrm{s}}^*}{\alpha_{\mathrm{l}}^*},\\ &D=\frac{D_{\mathrm{s}}^*}{D_{\mathrm{l}}^*},\quad c=\frac{c_{\mathrm{s}}^*}{c_{\mathrm{l}}^*},\quad k=\frac{m_{\mathrm{l}}}{m_{\mathrm{s}}},\\ &L_{\mathrm{e}}=\frac{\alpha_{\mathrm{l}}^*}{D_{\mathrm{l}}^*},\quad St=m_{\mathrm{l}}C_0\frac{c_{\mathrm{l}}^*}{L^*},\quad T_{\mathrm{equ}}=-St(1-C_{\mathrm{l}}) \end{aligned} \tag{1}$$

where the superscript (*) indicates a quantity with dimension, the subscripts (s) and (l) refer to the solid and liquid phases respectively, H is enthalpy, T is temperature, T_{f}^* is the fusion temperature of the pure solvent [K], l is an appropriate length dimension [m], L^* is the volumetric latent heat [J/m^3], c^* is the volumetric specific heat [J/m^3 K], c is the normalized specific heat, C^+ is solute concentration [wt%], C_0 is the initial solute concentration in the liquid, C is the concentration normalized by C_0, x is the space dimension in a one-dimensional domain, s is the location of the solid–liquid interface in this domain, t is time, α^* is thermal diffusivity [m^2/s], α is the normalized thermal diffusivity, D^* is mass diffusivity [m^2/s], D is the normalized mass diffusivity, k is the partition coefficient, m [K] is the slope of the assumed straight liquidus (l) or solidus lines (s) in the phase diagram (see Fig. 1), Le is the Lewis number, St is the solutal Stefan number, and T_{equ} is the dimensionless equilibrium temperature—read off the liquidus line in the phase diagram.

2.2. Governing equations

The problem set up involves a binary alloy melt at a uniform solute concentration $C_{\mathrm{l}}=1$ and uniform temperature T_0 held in a one-dimensional semi-infinite domain $0\leqslant x\leqslant\infty$. At time $t=0$ the temperature of the surface of this domain is fixed to a temperature T_{sur} sufficient to initiate solidification, so that, as time increases, a solid layer $x=s(t)$ grows from the $x=0$ surface into the liquid alloy. The governing equations are

Heat conduction in the solid:

$$\frac{\partial T}{\partial t}=\alpha\frac{\partial^2 T}{\partial x^2},\quad 0\leqslant x\leqslant s(t) \tag{2}$$

Heat conduction in the liquid:

$$\frac{\partial T}{\partial t}=\frac{\partial^2 T}{\partial x^2},\quad x\geqslant s(t) \tag{3}$$

Solute diffusion in the solid:

$$\frac{\partial C_{\mathrm{s}}}{\partial t}=\frac{1}{Le}D\frac{\partial^2 C_{\mathrm{s}}}{\partial x^2},\quad 0\leqslant x\leqslant s(t) \tag{4}$$

Solute diffusion in the liquid:

$$\frac{\partial C_{\mathrm{l}}}{\partial t}=\frac{1}{Le}\frac{\partial^2 C_{\mathrm{l}}}{\partial x^2},\quad x\geqslant s(t) \tag{5}$$

The boundary conditions are

at $x=0$

$$\frac{\partial C_{\mathrm{s}}}{\partial x}=0,\quad T=T_{\mathrm{sur}} \tag{6}$$

as $x\to\infty$

$$C_l\to 1,\quad T\to T_0 \tag{7}$$

On the moving solid–liquid interface $x=s(t)$ there is, due to the partitioning of the solute, a jump in solute concentration such that from the phase diagram, Fig. 1.

$$C_{\mathrm{s}}(s,t)=kC_{\mathrm{l}}(s,t)=kC^i(t) \tag{8}$$

where $C^i(t)$ is the liquid concentration on the interface. In addition, the temperature of the interface is given by the liquidus line, i.e.,

$$T^i(t)=T_{\mathrm{equ}}(s,t)=-St(1-C^i(t)) \tag{9}$$

Further, neglecting flow due to density change, the heat balance (Stefan condition) and mass balance on the moving solid–liquid interface at $x=s(t)$ are written as

$$c\alpha\left.\frac{\partial T}{\partial x}\right|_{\mathrm{s}^-}-\left.\frac{\partial T}{\partial x}\right|_{\mathrm{s}^+}=\frac{\mathrm{d}s}{\mathrm{d}t} \tag{10}$$

$$D\frac{1}{Le}\frac{\partial C_{\mathrm{s}}}{\partial x}-\frac{1}{Le}\frac{\partial C_{\mathrm{l}}}{\partial x}=(1-k)C_i\frac{\mathrm{d}s}{\mathrm{d}t} \tag{11}$$

2.3. Similarity solution

In a general solidification of a multi-component alloy due to segregation and curvature effects unique values of concentration and temperature cannot be associated with the solid–liquid interface, i.e., the values C^i and T^i will change with time. As noted by Rubinstein [12], however, in the binary-alloy problem—as described by the governing equations and boundary conditions given above—the interface concentration and temperature will take unique and constant values, C^i and T^i; a situation that allows

the governing equations to admit a closed form similarity solution. In brief, by setting

$$s = 2\lambda\sqrt{t} \tag{12}$$

the temperature and concentration profiles

$$T = T_{\text{sur}} + (T^i - T_{\text{sur}})\frac{\operatorname{erf}\left(\frac{1}{\sqrt{\alpha}}\frac{x}{2\sqrt{t}}\right)}{\operatorname{erf}\left(\frac{\lambda}{\sqrt{\alpha}}\right)},$$

$$C_s = kC^i, \quad 0 \leqslant x \leqslant s(t) \tag{13}$$

$$T = T_0 + (T^i - T_0)\frac{\operatorname{erfc}\left(\frac{x}{2\sqrt{t}}\right)}{\operatorname{erfc}(\lambda)},$$

$$C_l = 1 + (C^i - 1)\frac{\operatorname{erfc}\left(\frac{x\sqrt{Le}}{2\sqrt{t}}\right)}{\operatorname{erfc}(\lambda\sqrt{Le})} \quad x > s(t) \tag{14}$$

satisfy the heat and mass transport governing equations (2)–(5) along with the initial and fixed-boundary conditions. The three unknowns in these equations, C^i, T^i and λ, leading to a closed solution, are obtained on satisfying the condition set by the liquidus slope

$$T^i + St(1 - C^i) = 0 \tag{15}$$

and the heat (10) and mass (11) balance conditions on the moving interface $x = \text{s(t)}$

$$\sqrt{\pi}\lambda - c\sqrt{\alpha}\frac{T^i - T_{\text{sur}}}{\operatorname{erf}\left(\frac{\lambda}{\sqrt{\alpha}}\right)}\mathrm{e}^{-\frac{\lambda^2}{\alpha}} - \frac{T^i - T_0}{\operatorname{erfc}(\lambda)}\mathrm{e}^{-\lambda^2} = 0 \tag{16}$$

$$(1-k)C^i\lambda\sqrt{Le}\sqrt{\pi}\mathrm{e}^{\lambda^2 Le}\operatorname{erfc}(\lambda\sqrt{Le}) - (C^i - 1) = 0 \tag{17}$$

2.4. Constitutional under-cooling

Following Alexiades and Solomon [13], it is worthwhile to show the condition required for constitutional under-cooling. The equilibrium temperature at a given point in time and space is, by

$$T_{\text{equ}}(x,t) = -St(1 - C_l(x,t)) \tag{18}$$

An under-cooled liquid is defined as a liquid in which its actual temperature is below this equilibrium temperature, i.e., $T < T_{\text{equ}}$. In this inequality the temperature T can be expressed by the first part of (14) and the equilibrium temperature by the right-hand side of (18), written in terms of the interface temperature T^i by using the second part of (14) and (15). In this way the condition for under-cooling can be restated as

$$T_0 + (T^i - T_0)\frac{\operatorname{erfc}\left(\frac{x}{2\sqrt{t}}\right)}{\operatorname{erfc}(\lambda)} < T^i\frac{\operatorname{erfc}\left(\frac{x\sqrt{Le}}{2\sqrt{t}}\right)}{\operatorname{erfc}\left(\lambda\sqrt{Le}\right)} \tag{19}$$

Clearly, this condition is more likely to occur when the Lewis number is large Le—corresponding to a pronounced solute boundary layer ahead of the solid–liquid interface—and when the initial temperature is small. Further the likelihood of the condition occurring increase with distance x.

2.5. Limit solutions

Although traditionally the Rubinstein solution is presented under the condition that the initial temperature is above the initial liquidus, i.e., $T_0 > 0$ there is no reason why the initial liquid cannot be under-cooled so that $T_0 < 0$. In this case, as noted by Voller [20], two interesting limit solutions can be drawn from (12)–(17). In the first place if the partition coefficient is set to $k = 1$ the concentration remains fixed at $C = 1$ and (12)–(17) will reduce to the classic thermal problem of the one-dimensional solidification of an under-cooled pure melt reported in Carslaw and Jaeger [21]. Secondly, when the surface temperature is set to the interface temperature, $T_{\text{sur}} = T^i$, the solution (12)–(17) reduces to the solution for an under-cooled melt in an insulated domain; a solution that is useful for verifying simulations of equiaxed crystal growth in under-cooled melts [19].

3. An enthalpy model for the binary-alloy solidification

The enthalpy model for the binary-alloy problem is developed from the model presented by Crowley and Okendon [14]. The major extensions are a treatment that will allow for an under-cooled melt and problems that involve different specific heats in the solid and liquid phases. The key to the approach is to introduce three new variables the enthalpy defined as

$$H = \begin{cases} T + 1 & \text{if } f = 1 \\ T_{\text{equ}} + f & \text{if } 0 < f < 1 \\ T_{\text{equ}} + c(T - T_{\text{equ}}) & \text{if } f = 0 \end{cases} \tag{20}$$

where $0 \leqslant f \leqslant 1$ is the liquid fraction, the mixture solute defined by

$$C^f = fC_l + (1 - f)C_s \tag{21}$$

and the solute-potential defined by

$$V = \frac{C^{\text{f}}}{f(1-k) + k} \tag{22}$$

With the additional mixture definitions $\alpha^f = f + (1-f)c\alpha$ and $D^{\text{f}} = \frac{1}{Le}[f + k(1-f)D]$, single domain governing equations for heat and mass transport can be constructed, viz

$$\frac{\partial H}{\partial t} = \nabla(\alpha^{\text{f}}\nabla T), \quad x > 0 \tag{23}$$

$$\frac{\partial C^f}{\partial t} = \nabla(D^f\nabla V), \quad x > 0 \tag{24}$$

These are essentially the governing equations presented by Crowley and Ockendon [14] but with an extended definition of the enthalpy H and α^f in terms of the liquid fraction to allow for (i) the treatment of under-cooling and (ii) a jump in the specific heat. Note when $f = 0$ the solid phase transport Eqs. (2) and (4) are recovered from (23) and (24) and when $f = 1$ the liquid phase equations (3) and

(5) are recovered. Further, as noted by Crowley and Ockendon [14] (24) is the solute equivalent of the enthalpy equation (23); C^f, taking the role of enthalpy, jumps across the solid–liquid interface and, V, taking the role of temperature, is piecewise continuous across the interface.

4. The numerical solution

The key contribution of this work is to construct a new solution for (20)–(24) and verify its performance with the similarity solution. The novel features in this enthalpy solution are an ability to deal with a jump in the specific heat and under-cooling in the liquid. Note to retain generality in the solution developed it will not be assumed that the interface temperature and concentration are constants as specified in the Rubinstein similarity solution. Rather the developed enthalpy solution will allow the interface concentrations and temperatures to vary. In this way (i) a generality of application is maintained and (ii) obtaining a match between the new numerical enthalpy solution and similarity solution is seen as a stringent test.

An explicit time stepping solution of (20)–(24) is used. As illustrated in Fig. 3, the domain is covered by a one-dimensional array of 150 equally sized control volumes of length $\Delta x = 0.5$, a node point is located in the center of each volume, the left face of the first volume coincides with $x = 0$, a time step of $\Delta t = 0.025$ is used. The choice of space step is sufficient to satisfy grid independence and the choice of time steps is sufficient to avoid stability problems. At the start of the calculation all node values are set to $f_i = 1$, $C_i^f = 1$, $T_i = T_0$, $V_i = 1$ and $H_i = T_i + 1$. In order to initiate solidification in volume $i = 1$ the resetting $f_i = 0.999$ is made before time step calculations commence. Calculations are carried out until the solid–liquid interface has reached node $i = 20$ ($s = 9.75$). Following standard practice with enthalpy methods, see Price and Slack [4] and Voller and Cross [5] the calculated nodal fields of interest are recorded and output whenever the solid–liquid interface passes over a node point, i.e., when the condition $f_i^{\text{new}} < 0.5$ and $f_i > 0.5$ is met.

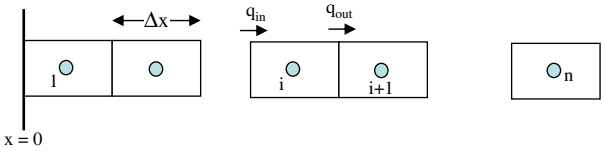

Fig. 3. Schematic of numerical grid arrangement.

Within a time step the solution operates as follows:

1. Nodal fields of enthalpy and mixture concentration are calculated from

$$H_i^{\text{new}} = H_i + \frac{\Delta t}{\Delta x^2}[q^H_{i\_\text{in}} - q^H_{i\_\text{out}}],$$
$$C_i^{f\_\text{new}} = C_i^f + \frac{\Delta t}{\Delta x^2}[q^C_{i\_\text{in}} - q^C_{i\_\text{out}}] \tag{25}$$

where assuming that the "out" face, on the right of volume i, retains liquid properties up until the volume is fully solid ($f_i = 0$) (the so-called "state of face approach" [22]), the fluxes in (25) are calculated as

$$q^H_{i\_\text{out}} = \begin{cases} T_i - T_{i+1}, & f_i > 0 \\ c\alpha(T_i - T_{i+1}), & \text{otherwise} \end{cases},$$
$$q^H_{i\_\text{in}} = q^H_{i-1\_\text{out}}, \quad q^H_{1\_\text{in}} = 2c\alpha(T_{\text{sur}} - T_1), \quad q^H_{n\_\text{out}} = 0 \tag{26}$$

$$q^C_{i\_\text{out}} = \begin{cases} \frac{1}{Le}(V_i - V_{i+1}), & f_i > 0 \\ \frac{Dk}{Le}(V_i - V_{i+1}), & \text{otherwise} \end{cases},$$
$$q^C_{i\_\text{in}} = q^C_{i-1\_\text{out}}, \quad q^C_{1\_\text{in}} = 0, \quad q^C_{n\_\text{out}} = 0 \tag{27}$$

2. Following the calculation of the enthalpy and mixture concentration fields the nodal liquid fraction field is updated. This update is only activated at phase change nodes, identified by the nodal liquid fraction falling strictly in the range $0 < f_i < 1$. At a phase change node the middle component of (20) gives

$$H_i^{\text{new}} = T_{i\_\text{equ}} + f_i^{\text{new}} \tag{28}$$

where interpreting V_i^{new} as the liquid phase concentration

$$T_{i\_\text{equ}} = -St(1 - V_i^{\text{new}}) \tag{29}$$

combining (28) and (29) and using the definition of V in (22) results in a quadratic equation in the node liquid fraction, the required positive root is given by

$$f_i^{\text{new}} = -\frac{-[k - (1-k)(H_i^{\text{new}} + St)] + \sqrt{[k - (1-k)(H_i^{\text{new}} + \text{St})]^2 - 4(1-k)(-kSt - kH_i^{\text{new}} + StC_i^{f\_\text{new}})}}{2(1-k)} \tag{30}$$

This calculation is caped by $f = \min(1, \max(0, f))$ to ensure that calculated liquid fractions remain in the range $0 \leqslant f \leqslant 1$. In more general problems the non-linear coupling between the liquid fraction, enthalpy and equilibrium temperature may require at iterative treatment as oppose to the quadratic solution presented here.

3. With the updated liquid fraction in hand, updated solute-potential and equilibrium temperature nodal fields can be calculated from (22) and (29), respectively.
4. The temperature field can be updated by inverting (20), i.e,

$$T_i^{\text{new}} = \begin{cases} H_i^{\text{new}} - 1, & \text{if } f = 1 \\ T_{\text{equ\_i}} & \text{if } 0 < f < 1 \\ \frac{H_i^{\text{new}} + (c-1)T_{\text{equ}}}{c} & \text{if } f = 0 \end{cases} \tag{31}$$

5. Finally, to allow the phase change to move from one volume to the next, at the end of the time step calculations a sweep is made through the nodal domain and the setting $f_{\text{i}}^{\text{new}} = 0.999$ made at all nodes i, where $f_i = 1$ with at least one neighboring node $f_{\text{nb}}^{\text{new}} = 0$.

On first glance the solution procedure may appear similar to that used by Crowley and Okendon [14]. The subtle and critical difference in the current method, however, is the identification of the phase change nodes through the liquid fraction value falling in the strict range $0 < f < 1$. Crowley and Okendon [14] identify the phase change nodes by the dimensionless enthalpy falling in the strict range $T_{\text{equ}} < H < T_{\text{equ}} + 1$. Although the later approach handles the movement of the solid–liquid interface between nodes automatically it is unable to deal with problems where the specific heat is discontinuous between phases and cannot solve problems where the liquid is under-cooled—a case where a number of nodal enthalpies will fall in the phase change range. In contrast, the former, proposed method based on liquid fraction identification can readily deal with a specific heat change and under-cooling. The small downside in this approach is the need to force the movement of the interface between nodes; but in practice—see step 5 in the above algorithm—such a forcing is easy to apply.

Within this discussion of alternative methods it needs to be pointed out that the enthalpy based approach of Wilson et al. [15] is also able to handle a jump in specific heat between the solid and liquid phases and an under-cooled liquid. This approach, however is aimed at a macroscopic treatment of the binary-alloy solidification and in the presence of an under-cooled liquid a mushy region is established where, in a one-dimensional domain, a fractional value of the liquid fraction $0 < f < 1$ is spread over several node points. In contrast, the enthalpy method developed here operates at the scale of the interface and assumes that a sharp interface (only one node in the range $0 < f < 1$) is maintained, even in the presence of under-cooling. Recall in the introduction the argument is made that if the scale (the thickness of the domain normal to the growth direction) is smaller than the critical wave length for morphological instability [17] a plane sharp interface can be maintained in the presence of an under-cooled liquid.

5. Results

Predictions with the proposed enthalpy method are made for the binary-alloy problem defined by the settings

$$T_{\text{sur}} = -1, \quad k = 0.1, \quad \alpha = 1.5, \quad c = 2,$$
$$D = Le, \quad St = -0.1 \tag{31a}$$

$$T_0, Le = \begin{cases} 0.1, 0.5 & \text{no undercooling} \\ 0.1, 4.0 & \text{constitutional undercooling} \\ -0.4, 0.5 & \text{imposed undercooling} \end{cases} \tag{31b}$$

Note in comparing with the Rubinstein solution, since the solute concentration in the solid phase will take a fixed constant value, the choice of solid mass diffusivity has no influence. As such, the setting of $D = Le$ is made to ensure that stability of the discrete solute transport equation is met as the Lewis number Le is increased.

Figs. 4–6 compare predictions from the proposed enthalpy solution with the Rubinstein solution. Each figure shows results for (a) the interface, (b) the actual and equilibrium temperature profiles when the interface has advanced to $s = 9.75$, (c) the concentration history for the 10^{th} node point, $x = 4.75$, and (d) the temperature history at $x = 4.75$. Fig. 4 corresponds to the case where there is no under-cooling in the liquid, Fig. 5 to the case where constitutional under-cooling occurs, and Fig. 6 to the case where an initial under-cooling is imposed; in all plots the numerical results are shown as symbols and the analytical as continuous lines. The following comments are made: In all cases the agreement between the numerical and analytical results is excellent. The region of constitutional under-cooling is clearly predicted—panel (b) in Fig. 5. In the imposed under-cooling case, Fig. 6, the warmest temperature is always at the interface, i.e., the solidification is driven by heat flowing into both the liquid and the solid.

In providing a more in-depth discussion about the results in Figs. 4–6 two comments are made about the predictions of the flat equilibrium temperature profile in the solid phase. Firstly, it is noted that the equilibrium temperature is directly connected to the concentration via the last component in (1). This value should not be confused with a real temperature and the appearance of a flat equilibrium temperature profile in the solid does not imply or require an infinite heat removal through the solid. Secondly, the flat (constant) prediction of the equilibrium temperature in the solid indicates that, for the choice of boundary condition at $x = 0$ (6), the predicted concentration at which the phase change occurs remains fixed throughout the solidification. It is stressed that this condition occurs naturally in both the analytical and numerical solutions, i.e., it is not imposed or assumed a priori. Because of the natural appearance of a flat concentration (equilibrium temperature) in the solid, as noted above, the exact choice of the solid diffusivity D in the numerical solution should not influence the concentration predictions. In practice, however, it is found that for small, but physically reasonable, values $D \sim 0.01$ there is a short range (3–5 nodes) in the numerical solution over which the predicted concentration value ramps to the fixed analytical value; once this region is

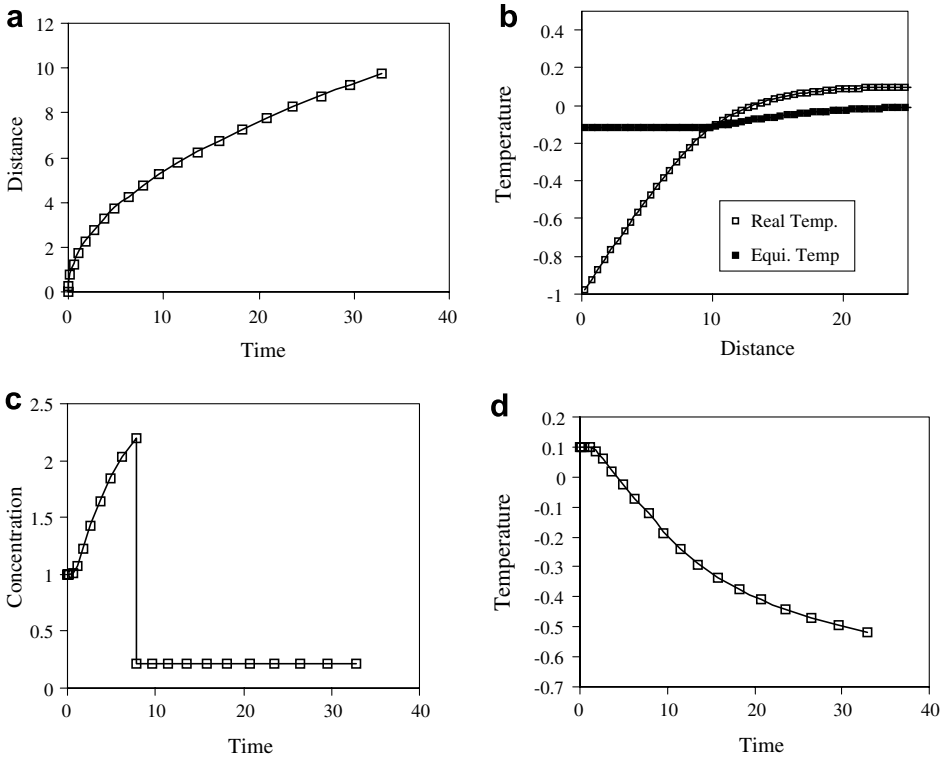

Fig. 4. Results for non under-cooling case, symbols are numeric results lines are analytical. (a) Interface movement $s(t)$, (b) temperature profiles when $s = 9.75$, (c) concentration history at $x = 4.75$, (d) temperature history at $x = 4.75$.

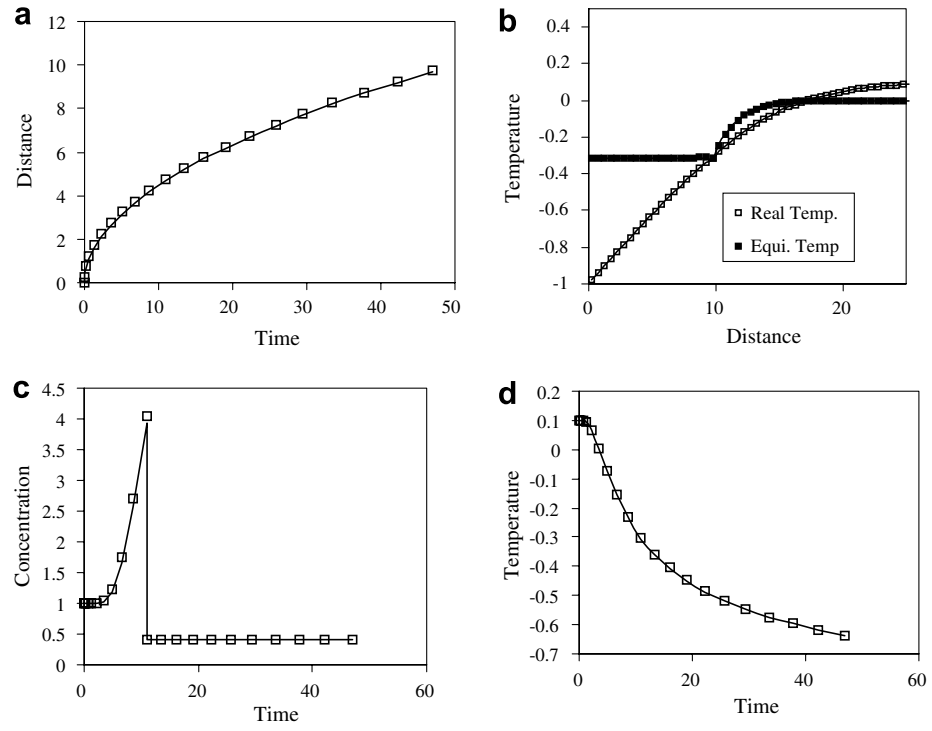

Fig. 5. Results for compositional under-cooling case, symbols are numeric results lines are analytical. (a) Interface movement $s(t)$, (b) temperature profiles when $s = 9.75$, (c) concentration history at $x = 4.75$, (d) temperature history at $x = 4.75$.

cleared the fidelity between the numerical and analytical solution is retained in all predicted fields.

If a different temperature boundary condition is employed at $x = 0$, e.g., the convective condition

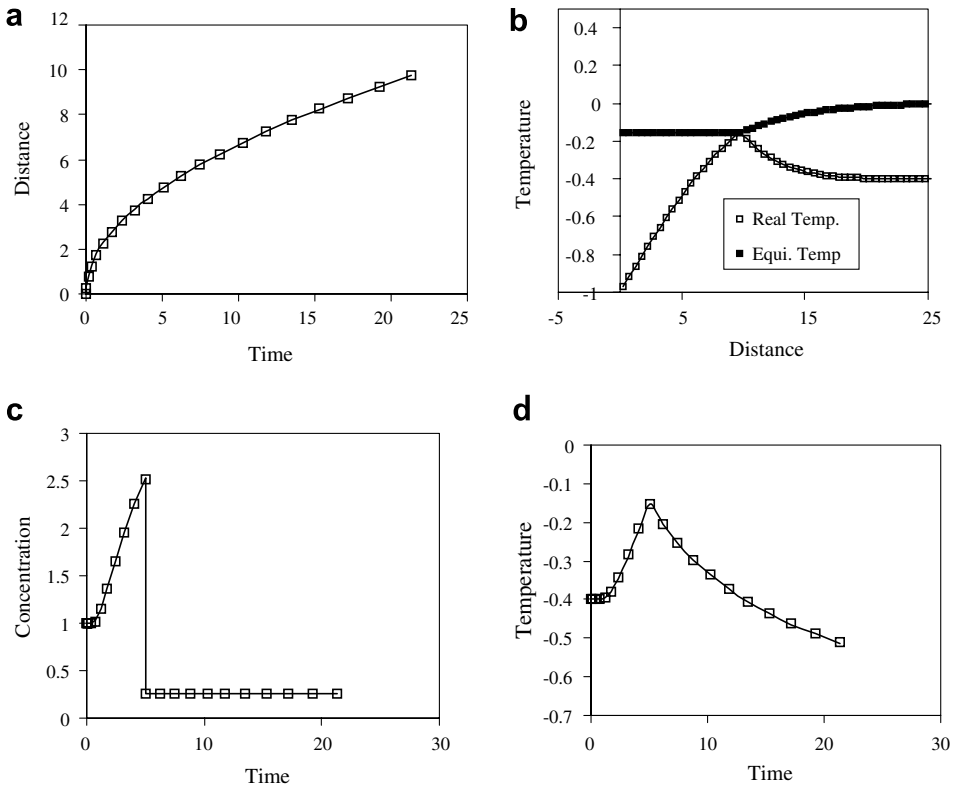

Fig. 6. Results for initial under-cooling case, symbols are numeric results lines are analytical. (a) Interface movement $s(t)$, (b) temperature profiles when $s = 9.75$, (c) concentration history at $x = 4.75$, (d) temperature history at $x = 4.75$.

$$c\alpha\frac{\partial T}{\partial x} = h(T_{\text{sur}} - T_{\text{amb}}) \tag{32}$$

where h a dimensionless convective transport coefficient and T_{amb} is the dimensionless ambient temperature, then a similarity solution cannot be found and a constant concentration field in the solid would not be expected. To see this, (32) is incorporated into the numerical solution and a prediction made with the settings

$$h = 1, \quad T_{\text{amb}} = -1, \quad T_0 = 0.1, \quad k = 0.1, \quad \alpha = 1.5,$$
$$c = 2, \quad Le = 4, \quad D = 0.01, \quad St = -0.1$$

The top panel of Fig. 7 shows predicted temperature and equilibrium temperature profiles when the solidification front is located at $s = 9.75$. Due to the relatively small value of D used in this case, concentrations at a point in the solid remain close to the value that existed when that point first formed. Hence, the equilibrium temperature profile in the solid provides a record of the interface temperature. The results clearly show a decrease in this value as the solidification front advances; a prediction in contrast to the previous results in Figs. 4–6 where this value remains fixed.

Up to this point the value of the Lewis number used as been relatively small. To redress this, the lower panel of Fig. 7 provides temperature predictions for a case identical to the top panel but with $Le = 100$; a number approaching those found in metal alloys. The Lewis number is the ratio of thermal to solute diffusivities. An increase in the Lewis number leads to a relative decrease in the width of the solute boundary layer ahead of the solidification front. This in turn leads to a steeper rise in the equilibrium temperature and the larger under-cooled region shown in the lower panel of Fig. 7.

6. Conclusions

There is current interest in modeling crystal growth processes in alloys [19,23–28]. These models require the tracking of a sharp solid–liquid interface—driven by coupled heat and mass transport—in the presence of an under-cooled liquid. A well known related test problem in the existing literature [12–16] is a one-dimensional solidification controlled by coupled heat and mass transport—the binary-alloy problem. Prior numerical solutions of the binary-alloy problem, however, steer clear of cases of a sharp interface in the presence of liquid under-cooling. The previous solutions either ignore cases where under-cooling will occur [14,15] or allow for the formation of a mushy region (a non-sharp front) when and under-cooled condition is reached [16]. In this paper, the binary-alloy problem as introduced by Rubinstein [12] is revisited and specific focus is placed on solutions of the problem in the presence of liquid under-cooling. In the first place an argument has been presented to show that—under appropriate restrictions on the width of the one-dimensional domain—physically realistic problems that involve a plane solid–liquid

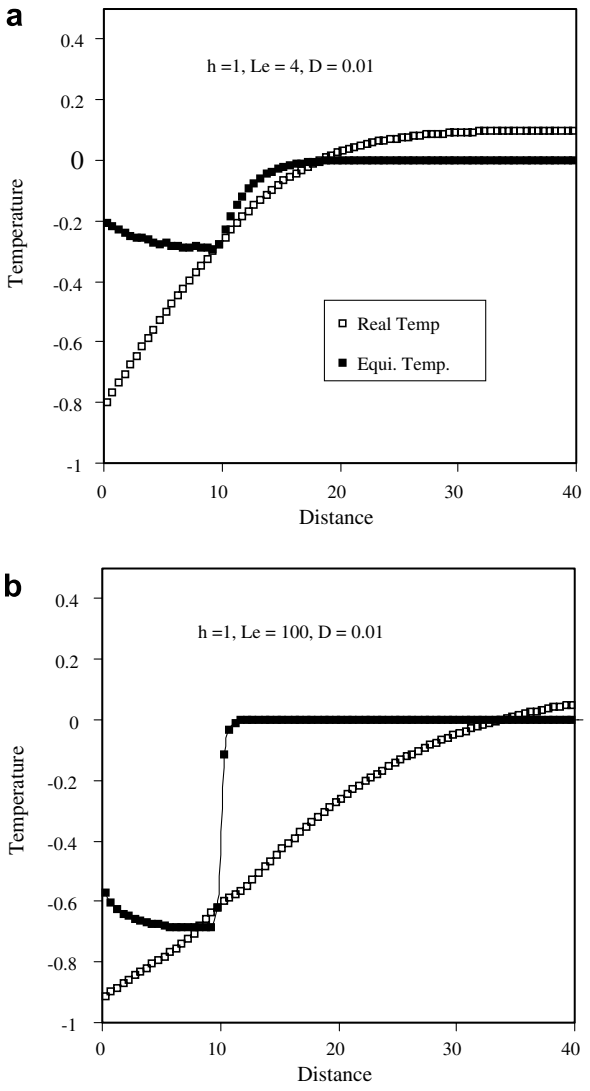

Fig. 7. Real and equilibrium temperatures profiles with convective cooling. Conditions are identical with Fig. 5 accept where noted on plot.

interface in the presence of liquid under-cooling may be realized. This is followed by the development of a novel numerical solution—based on the enthalpy based binary-alloy model proposed by Crowley and Okendon [14]—that is able to both (i) track a sharp solid–liquid interface for the binary-alloy problem in the presence of an under-cooled liquid, and (ii) handle changes in specific heat between the solid and liquid phases.. The author is unaware of previous fixed grid or enthalpy based solutions that are able to simultaneously handle these features. The performance of the proposed enthalpy method is compared with the available analytical solution. Across a range of conditions, spanning from no-under-cooling to an initially imposed under-cooling, the level of performance in predicting front movement, concentrations and temperature is, without exception, excellent. This underscores the potential strength of enthalpy models and solutions in solving current crystal growth problems of interest.

In terms of extensions of the method developed here. There are no intrinsic features in the proposed enthalpy solution scheme that will inhibit its immediate application in the solution of multi-dimensional problems. A caveat in such a case, however, is to be aware of the fact that if a sharp interface is assumed under-cooling associated with the curvature and speed of the interface may need to be included. The inclusion of these features can be based on recently reported enthalpy methods of equiaxed dendritic growth in under-cooled melts [19,25–28].

References

[1] J. Crank, Free and Moving Boundary Problems, Claendon Press, Oxford, 1984.
[2] V.R. Voller, Numerical methods for phase-change problems, in: W.J. Minkowycz, E.M. Sparrow, J.Y. Murthy (Eds.), Handbook of Numerical Heat Transfer, John Wiley, New York, 2006, pp. 593–622.
[3] N.R. Eyres, D.R. Hartree, J. Ingham, R. Jackson, R.J. Sarjant, S.M. Wagstaff, The calculation of variable heat flow in solids, Phil. Trans. R. Soc. A 240 (1946) 1–57.
[4] P.H. Price, M.R. Slack, The effect of latent heat on numerical solutions of the heat flow equation, Br. J. Appl. Phys 5 (1954) 285–287.
[5] V. Voller, M. Cross, Accurate solutions of moving boundary problems using the enthalpy method, Int. J. Heat Mass Transfer 24 (1981) 545–556.
[6] A.W. Date, Novel strongly implicit formulation for multidimensional Stefan problems, Numer. Heat Transfer B 27 (1992) 231–251.
[7] M. Lacroix, V.R. Voller, Finite difference solutions of solidification phase change problems: transformed vs. fixed grids, Numer. Heat Transfer 17 (1990) 25–42.
[8] R. Giffith, B. Nassersharif, Comparison of one-dimensional interface-following and enthalpy methods for the numerical solution of phase change, Numer. Heat Transfer (B) 18 (1990) 169–187.
[9] J. Caldwell, C.-C. Chen, Numerical solutions of the Stefan problem by the enthalpy methods and the heat balance integral method, Numer. Heat Transfer B 33 (1998) 99–117.
[10] V.R. Voller, A. Mouchmov, M. Cross, An explicit method for coupling temperature and concentration fields in solidification models, Appl. Math. Model. 28 (2004) 79–94.
[11] S. Ganguly, S. Chakraborty, A generalized enthalpy-based macro model for ternary alloy solidification simulations, Numer. Heat Transfer B 51 (2007) 293–313.
[12] L. Rubinstein, The Stefan Problem, Translations of Math. Monographs, vol. 27, American Mathematical Society, Providence, 1971.
[13] V. Alexiades, A.D. Solomon, Mathematical Modeling of Melting and Freezing Processes, Hemisphere, Washington, 1984, pp. 106–109.
[14] A.B. Crowley, J.R. Ockendon, On the numerical solution of an alloy solidification problem, Int. J. Heat Mass Transfer 22 (1979) 941–947.
[15] V.R. Voller, An implicit enthalpy solution for phase change problems: with application to a binary alloy solidification, Appl. Math. Model. 11 (1987) 110–116.
[16] D.G. Wilson, A.D. Solomon, V. Alexiades, A model of binary alloy solidification, Int. J. Numer. Meth. Eng. 20 (1984) 1084–1967.
[17] W. Kurz, D.J. Fisher, Fundamentals of Solidification, Trans Tech Publishing, Switzerland, 1986, pp. 53–54.
[18] W.W. Mullins, R.F. Sekerka, Stability of a planar interface during solidification of a dilute binary alloy, J. Appl. Phys. 35 (1964) 444–451.
[19] V.R. Voller, An enthalpy method for modeling dendritic growth in a binary alloy, Int. J. Heat and Mass Transfer, in press, doi:10.1016/j.ijheatmasstransfer.2007.04.025.
[20] V.R. Voller, A similarity solution for solidification of an under-cooled binary alloy, Int. J. Heat Mass Transfer 49 (2006) 1981–1985.

[21] H. Carslaw, J. Jaeger, Conduction of Heat in Solids, second ed., Clarendon Press, Oxford, 1959.
[22] V.R. Voller, Numerical treatment of rapidly changing and discontinuous conductivities, Int. J. Heat Mass Transfer 44 (2001) 4553–4556.
[23] J.C. Ramirez, C. Beckermann, A. Karma, H.-J. Diepers, Phase-field modeling of binary alloy solidification with coupled heat and solute diffusion, Phys. Rev. E 69 (2004).
[24] P. Zhao, M. Vénere, J.C. Heinrich, D.R. Poirier, Modeling dendritic growth of a binary alloy, J. Computat. Phys. 188 (2003) 434–461.
[25] V.R. Voller, An enthalpy based scheme for simulating dendritic growth, in: C.-A. Gandin, M. Bellet (Eds.), Modeling of Casting, Welding and Advanced Solidification Processes-XI, TMS, Warrendale, 2006, pp. 465–472.
[26] V.R. Voller, N. Murfield, Application of an enthalpy method for dendritic solidification, in: A.J. Novak et al. (Eds.), Numerical Heat Transfer 2005, Institute of Thermal Technology, Poland, 2005, pp. 379–386.
[27] D. Chatterjee, S. Chakraborty, A hybrid lattice Boltzmann model for solid–liquid phase transition in presence of fluid flow, Phys. Lett. A 351 (2006) 359–367.
[28] D. Pal, J. Bhattacharya, P. Dutta, S. Chakraborty, An enthalpy model for simulation of dendritic growth, Numer. Heat Transfer B 50 (2006) 59–78.